



## Obrabotka metallov -

## Metal Working and Material Science

Journal homepage: [http://journals.nstu.ru/obrabotka\\_metallov](http://journals.nstu.ru/obrabotka_metallov)








### Investigation of cutting forces and machinability during milling of corrosion-resistant powder steel produced by laser metal deposition





Artem Babaev<sup>1,a,\*</sup>, Victor Kozlov<sup>2,b</sup>, Artem Semenov<sup>1,c</sup>, Anton Shevchuk<sup>1,d</sup>, Valeriia Ovcharenko<sup>2,e</sup>,  
Evgeniy Sudarev<sup>2,f</sup>

<sup>1</sup> National Research Tomsk State University, 36 Lenin Avenue, Tomsk, 634050, Russian Federation

<sup>2</sup> National Research Tomsk Polytechnic University, 30 Lenin Avenue, Tomsk, 634050, Russian Federation

<sup>a</sup>  <https://orcid.org/0000-0003-2334-1679>,  [temkams@mail.ru](mailto:temkams@mail.ru); <sup>b</sup>  <https://orcid.org/0000-0001-9351-5713>,  [kozlov-viktor@bk.ru](mailto:kozlov-viktor@bk.ru);

<sup>c</sup>  <https://orcid.org/0000-0002-8663-4877>,  [artems2102@yandex.ru](mailto:artems2102@yandex.ru); <sup>d</sup>  <https://orcid.org/0009-0003-5272-4350>,  [shvpro@yandex.ru](mailto:shvpro@yandex.ru);

<sup>e</sup>  <https://orcid.org/0009-0000-4797-5604>,  [vag14@tpu.ru](mailto:vag14@tpu.ru); <sup>f</sup>  <https://orcid.org/0000-0002-5596-4048>,  [sudarev@tpu.ru](mailto:sudarev@tpu.ru)

#### ARTICLE INFO

##### Article history:

Received: 11 March 2024

Revised: 30 March 2024

Accepted: 09 April 2024

Available online: 15 June 2024

##### Keywords:

Milling

Cutting forces

Roughness

Laser Metal Deposition

Cutting modes

##### Funding

The work was carried out with financial support from the Russian Science Foundation, project No. 23-79-10166 (<https://rscf.ru/en/project/23-79-10166>). The authors express their gratitude to the Russian Science Foundation for funding this work.

#### ABSTRACT

**Introduction.** Additive manufacturing technologies for the production of geometrically approximate workpieces require post-processing. This applies to the use of cutting tools in milling operations when machining critical surfaces. The latter are specified strict requirements to accuracy of linear and angular dimensions and quality of the surface layer. An urgent task remains to increase machining productivity when recording cutting forces and surface roughness to develop technological recommendations. **Purpose of work:** experimental determination of cutting modes providing the highest productivity when milling *LMD*-workpieces (Laser Metal Deposition) made of steel *0.12-Cr18-Ni10-Ti (AISI 321)* by carbide end mill, while maintaining the milling cutter operability and required roughness. The properties and microstructure of the specimens along and across the build direction **are investigated**. The influence of feed (when the mill moves across and along the build direction), depth and width of milling, speed on the components of the cutting force and roughness of the machined surfaces during counter milling of *LMD*-workpieces made of steel *0.12-Cr18-Ni10-Ti (AISI 321)* with end mill made of *H10F* carbide with a diameter of 12 mm without wear-resistant coating is established and formalized. **The research methods** are the dynamic measurement of all three components of the cutting force using a three-component dynamometer and the measurement of roughness with a profilometer. The condition and microgeometry of the cutting edges were monitored before and after milling using scanning optical and scanning electron microscopy. **Results and Discussion.** The difference in cutting forces depending on the milling pattern (along and across the build direction) was shown. Studies showed that the milling depth and cutting speed have little effect on the lateral and axial components of the cutting force. The feed force increases significantly with increasing depth of cut, especially when feeding across the specimen build direction. It is found that all three components of the cutting force are directly proportional to the value of the minute feed. The equations for calculating all three components of the cutting force with a change in the minute feed are obtained.

**For citation:** Babaev A.S., Kozlov V.N., Semenov A.R., Shevchuk A.S., Ovcharenko V.A., Sudarev E.A. Investigation of cutting forces and machinability during milling of corrosion-resistant powder steel produced by laser metal deposition. *Obrabotka metallov (tekhnologiya, oborudovanie, instrumenty) = Metal Working and Material Science*, 2024, vol. 26, no. 2, pp. 38–56. DOI: 10.17212/1994-6309-2024-26.2-38-56. (In Russian).

## Introduction

The increase in the number of technologies and materials for additive manufacturing of blanks is accompanied by increased requirements for understanding the features of shaping of functional products, patterns and processes of subtractive processing [1]. Regardless of the additive technology used to produce the workpiece, the latter needs post-processing – thermal, chemical or using subtractive methods [2–4].

#### \* Corresponding author

Babaev Artem S., Ph.D. (Engineering), Senior researcher  
National Research Tomsk State University,  
36 Lenin Avenue,  
634050, Tomsk, Russian Federation  
Tel.: +7 952 805-09-26, e-mail: [temkams@mail.ru](mailto:temkams@mail.ru)

Heat treatment methods (annealing, normalization, etc.) allow to provide phase transformations in the metal structure, and also significantly affect the physical and mechanical characteristics of the workpiece material, and, as a result, the resistance to cutting [5–9].

In order to give the final shape, maintain geometric accuracy and surface roughness, the additive workpiece is subjected to subtractive processing, i.e. machining with the removal of material. The latter can include the processes of blade and abrasive cutting. At the same time, it is important to understand that the removal of “excess” material (overlap or allowance) is accompanied by a range of specific phenomena – chip formation, the occurrence and dynamic change of cutting forces, temperature changes in the cutting zone, the gradual formation of wear on the working surfaces of the cutting tool, etc. [10–21]. Special attention is paid to the peculiarities of the interaction of the “tool material-machined material” pair. Observation and study of these phenomena contribute to the development of scientifically based recommendations on the choice and assigning of edge cutting machining modes, especially when it comes to machining new materials or workpiece obtained by additive methods – it becomes possible to indirectly estimate the economic costs of producing a fully functional product [4].

Significant progress has been made in the synthesis of stainless steels by various additive methods, which makes it possible to use the resulting workpiece of stable quality for further heat treatment, as well as to give the required structural design, roughness, shape and size accuracy by removing the allowance [22–25]. In [26], a team of researchers studied the impact of additive manufacturing on the development of the space industry. The authors concluded that the repeatability and consistency of the mechanical properties of finished parts of additive manufacturing have not yet been fully studied, and special attention should be paid to the development of standards, certificates and inspection protocols.

Scientific papers [15, 27–29] are devoted to the anisotropy of the properties of additive metallic materials. In the review work [29], the main factors that cause microstructural features and heterogeneity of mechanical properties are highlighted: grain morphology; crystallographic texture; defects in the absence of merger; phase transformations; heterogeneous recrystallization; banding of layers and microstructural coarsening. As a result, the anisotropy of the properties affects the resistance of the material to cutting.

It is necessary to know the distribution of contact stresses on the rake surface and on the wear chamfer of the flank and back surface to calculate the milling teeth for strength, in addition to the cutting forces  $P_z$ ,  $P_y$  and  $P_x$  acting on the milling tooth. The authors of [30] have developed a technique for constructing of a contact stresses diagram on the rake surface of the cutting wedge when turning steel, but it is also applicable in milling. The length of the chip contact with the rake surface of the milling cutter tooth at the largest cut thickness, i.e. for counter milling, this occurs at the moment preceding the tooth exhaust from contact with the workpiece should be known to do this. This contact length  $c$  can not only be measured, but also determined by graphs  $c = f(a, \gamma)$  [30], knowing the uncut chip thickness  $a$  (mm) at the end of the tooth contact with the workpiece:  $a_{max} \approx s_z \times 2 \times (t/d)^{1/2}$ , where  $s_z$  is the feed to the tooth, mm/tooth;  $t$  is the milling depth, mm;  $d$  is the diameter of the cutter, mm;  $\gamma$  is the rake angle of the cutting wedge.

### Designations (Nomenclature)

- $P_{laser}$  is the laser radiation power, W;
- $Dia_{laser}$  is the laser spot diameter, mm;
- $x_{width}$  is the width offset of the rollers, mm;
- $h_{width}$  is the height offset of the rollers, mm;
- $V_{LMD}$  is the LMD speed, mm/s;
- $Q_{powder}$  is the powder consumption, g/min;
- $\sigma_{0.2}$  is the yield strength, MPa;
- $\sigma_{UTS}$  is the ultimate tensile strength, MPa;
- $\delta_5$  is the relative elongation, %;
- $KCU$  is the impact strength, J/cm<sup>2</sup>;

$Ra$  is the arithmetic mean deviation of the roughness profile,  $\mu\text{m}$ ;

$d$  is the milling cutter diameter, mm;

$d_f$  is the diameter of the milling cutter shank, mm;

$l$  is the length of the working part of the milling cutter, mm;

$L$  is the full length of the milling cutter, mm;

$\alpha$  is the clearance(rear) angle, degree;

$\gamma$  is the rake angle, degree;

$\omega$  is the angle of inclination of the chip groove, degree;

$z$  is the number of teeth, pcs;

$\rho$  is the radius of rounding (sharpness) of the cutting edge,  $\mu\text{m}$ ;

$Ra(\rho)$  is the arithmetic mean deviation of the roughness profile on the cutting edge,  $\mu\text{m}$ ;

$\beta$  is the wedge angle, degree;

$t$  is the milling depth, mm;

$B$  is the milling width, mm;

$V$  is the cutting speed, m/min;

$n$  is the rotation speed, rpm;

$f_{\min}$  is the feed per minute, mm/min;

$Q$  is the volume of the material to be removed (cutting capacity),  $\text{mm}^3/\text{min}$ .

## Experiment technique

### *Specimen (shape, properties, structure)*

The workpiece (after its final preparation – the specimen) for testing was obtained using direct laser deposition technology (*LMD – Laser Metal Deposition*) from powder raw materials of the *Fe-Cr-Ni-Ti* system. Changes in the irradiation parameters (laser power, irradiation rate and the distance between layers) affect the size of the melt bath and the porosity of the structure of the resulting material, and, consequently, the mechanical properties of additively manufactured workpieces [31]. Therefore, the workpieces were obtained in the spent modes under the same conditions from the powder of the same delivery batch sequentially in the same modes (Table 1) and along the same deposition trajectory (Fig. 1).

The specimens were obtained by successive unidirectional filling vectors: feeding along the specimen at a  $V_{LMD}$  velocity, then feeding across the specimen by  $y = 1.67$  mm, and so on until the first layer was obtained. Then by moving to the thickness of one layer ( $h_{width} = 0.8$  mm), moving to the starting point of synthesis of the first layer, filling along the long side of the sample, etc.

All workpieces were obtained from a powder mixture, the passport and certified composition of which is given (Table 2).

The resulting workpieces after growing had dimensions of  $190 \times 100 \times 14$  mm. The crust on workpieces was removed by electroerosion cutting. The latter made it possible to eliminate the appearance of distortion of internal stresses on the machined surfaces.

Specimens for physical and mechanical tests were cut out of several workpieces. In order to avoid the spread of values caused by the location of the specimens relative to the workpiece, a check was carried

Table 1

### *LMD modes for steel 0.12-Cr18-Ni10-Ti (AISI 321) products manufacturing*

Steel	$P_{laser}$ , W	$Dia_{laser}$ , mm	$x_{width}$ , mm	$h_{width}$ , mm	$V_{LMD}$ , mm/s	$Q_{powder}$ , $\text{mm}^3/\text{min}$
0.12-Cr18-Ni10-Ti (AISI 321)	2,400	2.7	1.67	0.8	25	16

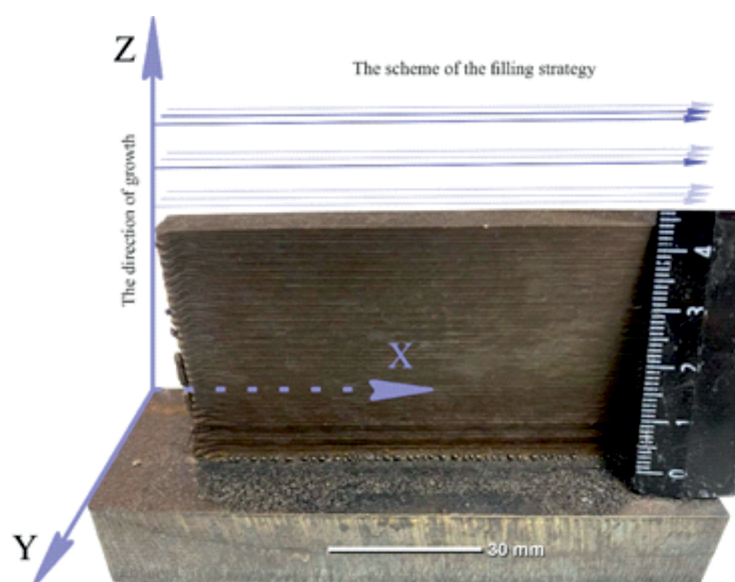


Fig. 1. Scheme of the filling strategy for growing specimens from steel 0.12-Cr18-Ni10-Ti (AISI 321)

Table 2

#### Chemical composition of the powder

Chemical element, mass %									
<i>Fe</i>	<i>Cr</i>	<i>Ni</i>	<i>Mn</i>	<i>Si</i>	<i>Ti</i>	<i>Cu</i>	<i>V</i>	<i>Mo</i>	<i>C</i>
Bal.	18.19	10.67	1.14	0.54	0.51	0.18	0.10	0.17	0.06

out – the location of the test specimens was determined and cut out randomly. The specimens were certified at room temperature using various research equipment. As a result, data on thermophysical and physical and mechanical properties were obtained (Table 3). The mechanical properties of steel 0.12-Cr18-Ni10-Ti (AISI 321) in its initial state and after heat treatment correspond to OST 95-29-72 “Workpieces made of corrosion-resistant steels”.

Blanks with a size of 160×80×8 mm were used directly for milling.

The thermophysical properties of steel 0.12-Cr18-Ni10-Ti (AISI 321) were determined at a temperature of 20 °C. The following values were obtained: density 7.91 g/cm<sup>3</sup>; thermal conductivity coefficient 14 W/m·°C; specific heat capacity 473 J/kg·°C.

Figure 2 shows the microstructure of the specimen in the ZY plane and in the ZX plane.

The study of the microstructure showed the two-phase nature of additive specimens: an austenitic matrix based on  $\gamma$ -Fe with a face-centered cubic lattice (FCC) and high-temperature rack and vermicular  $\delta$ -ferrite with a body-centered cubic lattice (BCC), which is also confirmed by a diffractogram of the specimens (Fig. 3). Mainly  $\delta$ -ferrite is formed at the fusion boundaries. Titanium carbides  $TiC$  are present in the specimens.

Table 3

#### Mechanical properties of steel 0.12-Cr18-Ni10-Ti (AISI 321)

Condition	Sampling direction (see Fig. 1)	Hardness, HB	$\sigma_{0.2}$ , MPa	UTS ( $\sigma_{UTS}$ ), MPa	$\delta_5$ , %	KCU, J/cm <sup>2</sup>
Plate (OST 95-29-72)	–	≈180–190	246	520	37	215–372
LMD	X axis	193–205	412±20	627±34	48.2±1.5	271±18
	Z axis		387±16	606±28	51.2±2	286±21



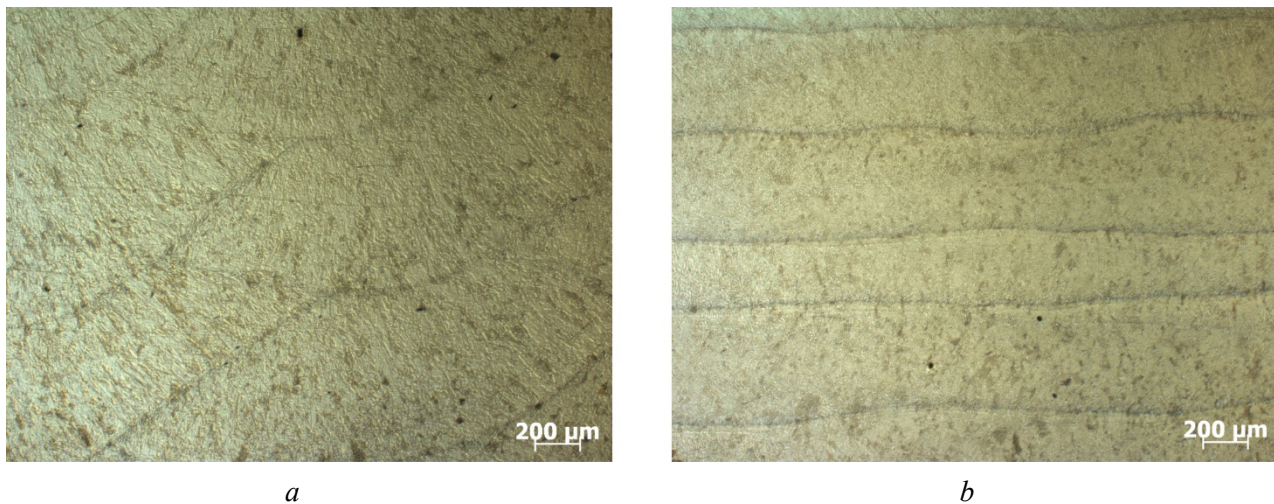


Fig. 2. Microstructure of the specimen in the ZY plane (a), in the ZX plane (b)

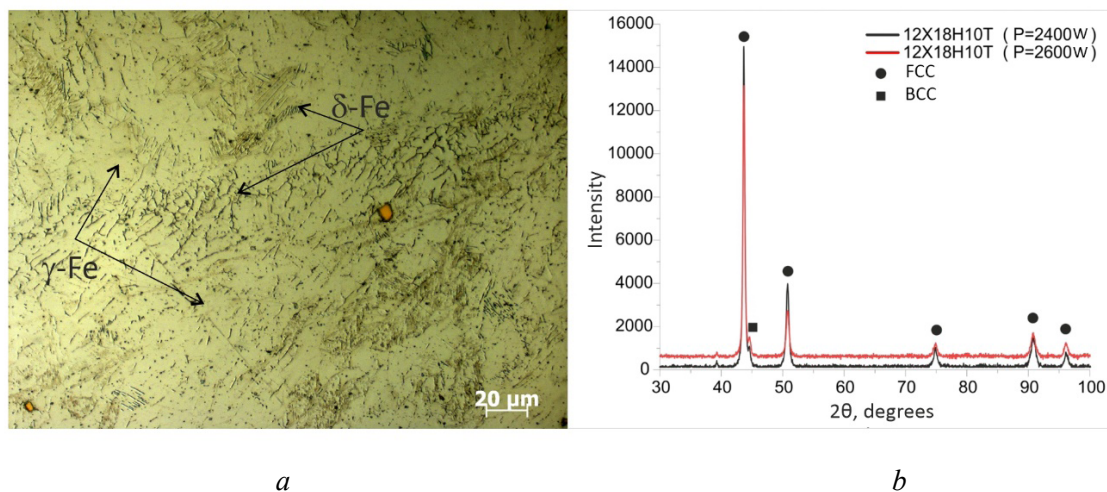


Fig. 3. Typical microstructure of LMD steel 0.12-Cr18-Ni10-Ti (AISI 321)

### The cutting tool and its geometry

Carbide end mills with universal geometry were used as cutting tools for machining steels from group **P** (Fig. 4) and (Table 4). The cemented carbide of the *H10F* brand had the following characteristics:  $\approx 89.4$  wt. % of tungsten carbide; up to 0.6 wt. % of mixed carbides and about 10.0 wt. % of cobalt as a binder. The grain size of the carbide phase is 0.5–0.6  $\mu\text{m}$ , the bending strength is  $\approx 3,200$  MPa, and the hardness is 92 *HRA*.

In total, 5 milling cutters were sequentially manufactured on a tool and cutter grinding machine without readjustment. The cemented carbide blanks for manufacturing were taken from one shipment. This made it possible to avoid the appearance of an undesirable factor — the influence of heterogeneity in the quality of the tool material. In order to avoid the effect of wear on the flank or back surface on the data obtained, milling cutters were used that worked to a wear chamfer length no more than 0.10–0.12 mm on the flank or back surface.

It is known that the parameters of microgeometry have a stable effect on the mechanics and dynamics of the cutting process, while changing the conditions of friction and wear of the cutting edge [21]. In order to avoid the appearance of this factor on the results of this work, the state of the microgeometry of the cutting edges were estimated. The *Edge Master X* device, manufactured by *Alicona* (Switzerland), was used to

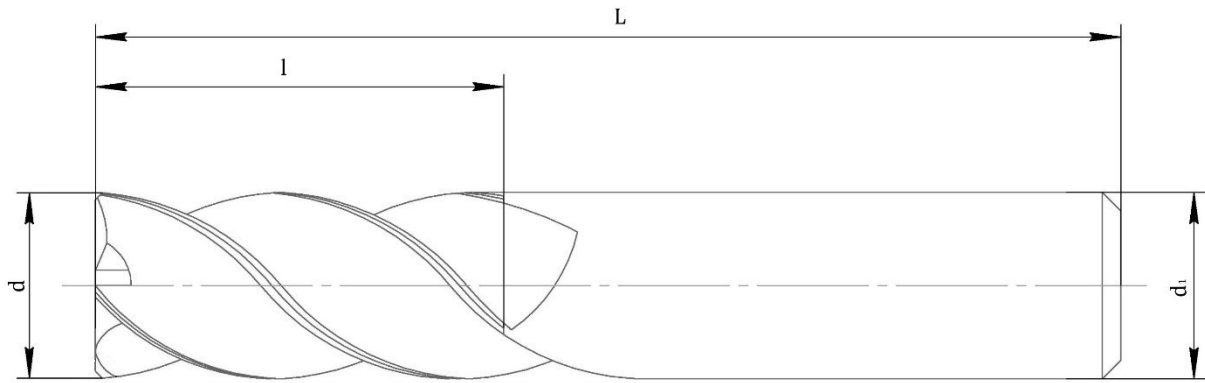


Fig. 4. Schematic representation of a mill with indication of the main geometric characteristics

Table 4

Values of the main geometric characteristics of the *H10F* carbide mill

$d$ , mm	$d_p$ , mm	$l$ , mm	$L$ , mm	$\alpha$ , degree	$\gamma$ , degree	$\omega$ , degree	$z$ , pcs
12	12h6	26	84	+10	+8	40	4

carry out measurements to understand the state of the microgeometry of the cutting edges. Measurements were made on all working edges located on the screw surface, while retreating from the end by 2–3 mm (Fig. 5).

#### Test bench and work plan

The tests were carried out on the milling machining center of the *DMU 50* model, manufactured by *DMG* (Germany). According to the passport data and production experience, the machine has a sufficiently high rigidity for roughing steel in modes with accelerated material removal. The maximum spindle speed  $n_{\max}$  is  $10,000 \text{ min}^{-1}$ , and the feed rate is up to  $30,000 \text{ mm/min}$ .

The specimen was fixed in a special device mounted within the bearing surface of the dynamometer (Fig. 6). Preliminary modeling of the grip conditions was carried out in order to prevent collisions during

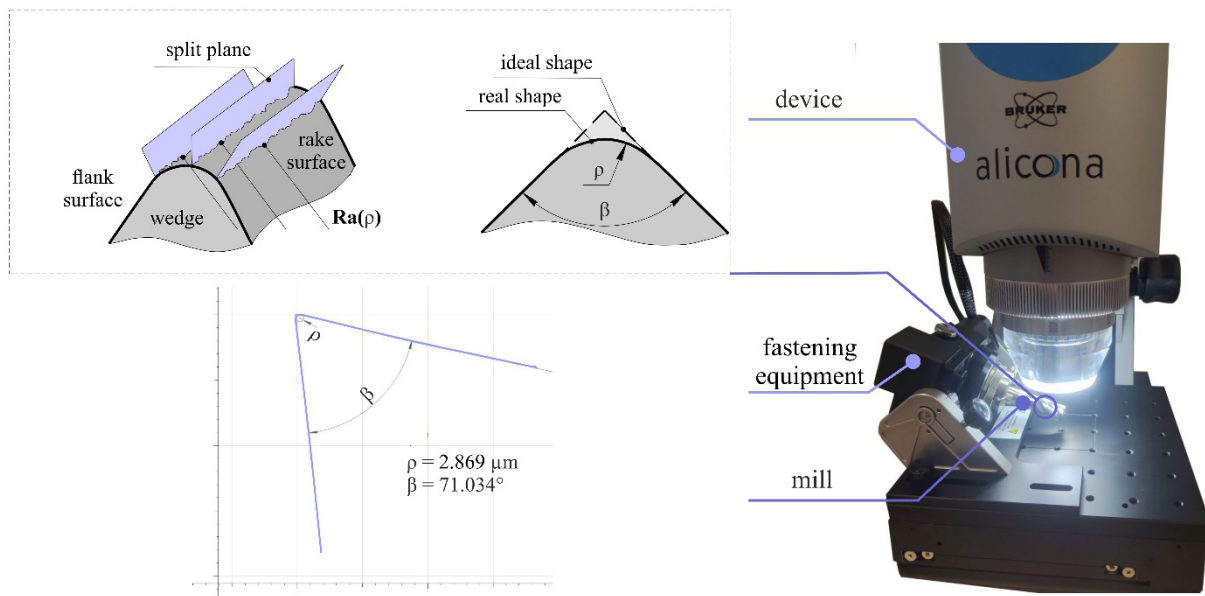


Fig. 5. Measuring circuit and example presentation of cutting edge microgeometry parameters

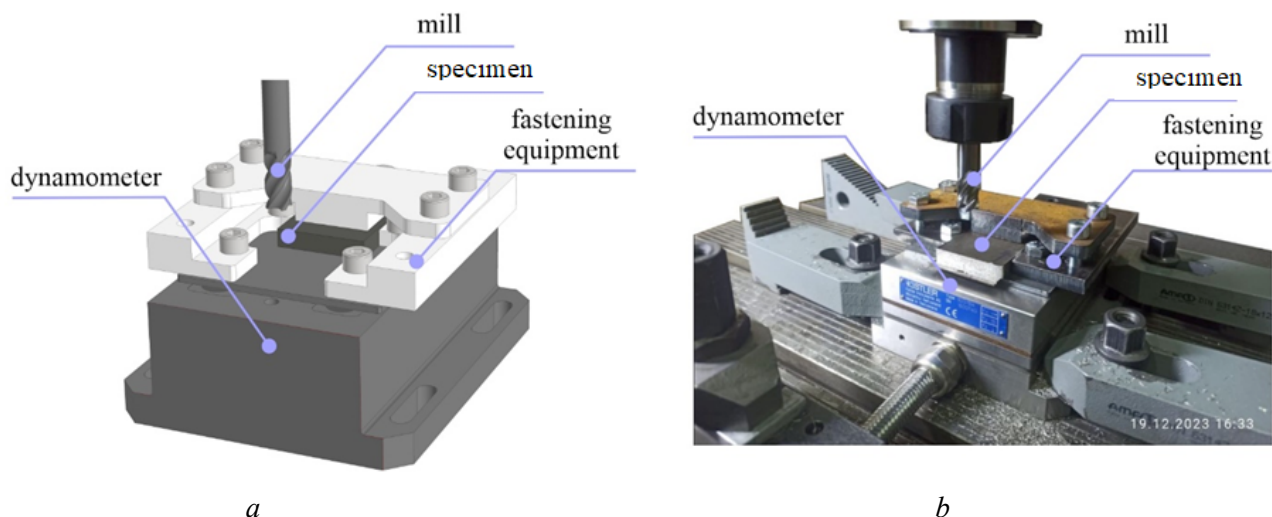


Fig. 6. Model (a) and appearance (b) of the experimental stand with an installed dynamometer, a specimen and a mill

testing. The *Kistler* dynamometer mod. 9257BA for measuring cutting forces was mounted directly on the table of the milling machine.

The specimens were milled both along and across the build direction (see Fig. 1). In this case, it is important to track the influence of the specimen build direction on the change in cutting forces and the roughness of the have machined surface. Milling was carried out without the use of a coolant to minimize the influence of the cooling factor and lubrication of the cutting zone. The cutting modes were adopted according to Table 5 in order to experimentally determine the highest possible feed according to the strength of the cutter and its teeth, that is, for the increased volume of the chip being cut  $Q$ .

Attempts to increase the cutting speed and feed above the table values inevitably led to the failure of the mill after the first seconds of operation (Fig. 7).

During the tests, conventional or up milling was used according to the scheme shown in Fig. 8.

A distinctive feature of conventional or up milling (counter milling) from climb or down milling (passing milling) is that during conventional milling, the uncut chip thickness  $a_i$  increases from zero to the maximum value at the moment the tooth leaves contact with the workpiece. This allows for a short period of time to ensure smooth loading of the cutting edge, unlike in climb milling, when there is an abrupt load in the first moments of cutting, often leading to premature destruction of the cutting edges.

Table 5

#### Milling modes

Experiment No.	$n$ , rev/min	$V$ , m/min	$F_{min}$ , mm/min	$t$ , mm	$B$ , mm	$Q$ , mm <sup>3</sup> /min
1	2.000	75	120	1	7	840
2			240			1.680
3			480			3.360
4			850	2		5.950
5						11.900
6						14.875
7	2.500	94	1.050	2.5		17.850
8				3		22.050
9						



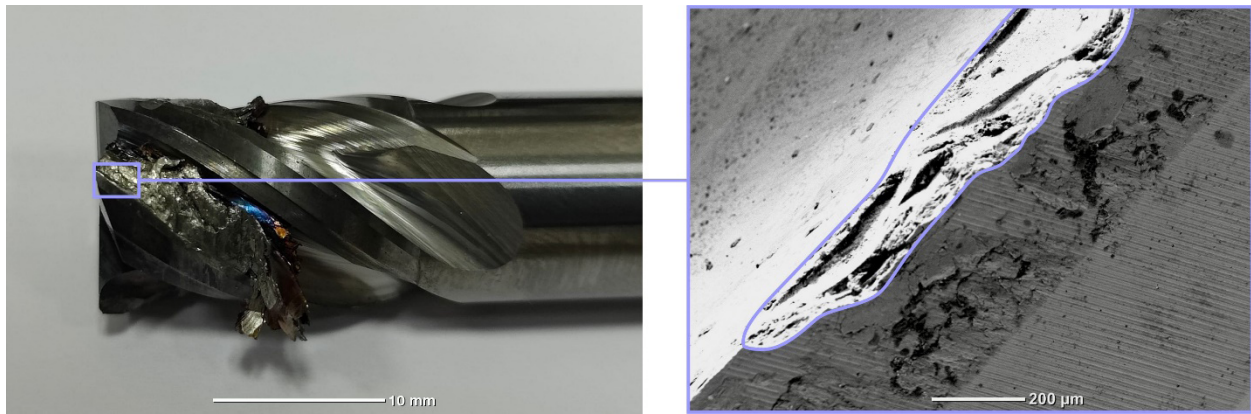


Fig. 7. Appearance of a mill prematurely removed from testing and a fragment of the cutting-edge wear

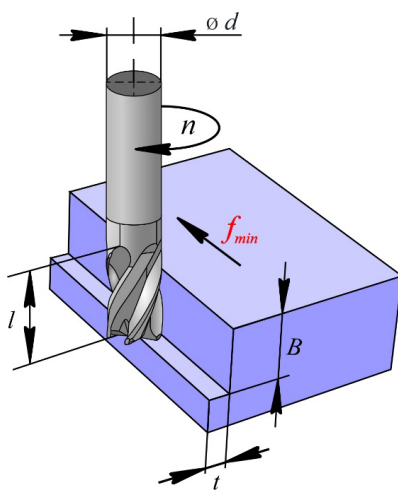


Fig. 8. Schematic representation of milling modes

The components of the cutting force were measured using a three-component dynamometer model 9257BA Kistler (Switzerland) (Fig. 9). The duration of the data collection cycle was 5 seconds from the moment of steady cutting, that is, after all the teeth of the milling cutter had already taken part in machining the specimen. The registration of forces was carried out with a frequency of 10 kHz signal reception.

The rotation of the milling cutter was always performed clockwise. In the built-in software of the Kistler dynamometer, the symbols  $F_z$  (tangential component of the cutting force, i.e. acting vertically downwards for conventional turning),  $F_x$  (axial component of the cutting force, i.e. acting in a horizontal plane along the axis of rotation of the lathe spindle from left to right for conventional turning),  $F_y$  (radial component of the cutting force, i.e. acting in a horizontal plane and perpendicular to the axis of rotation of the spindle of the lathe towards the operator for conventional turning) which indicate the direction of forces characteristic of classical turning. These symbols are indicated on the graphs of changes in these components on the dynamometer monitor. In Fig. 9, it is indicated by the

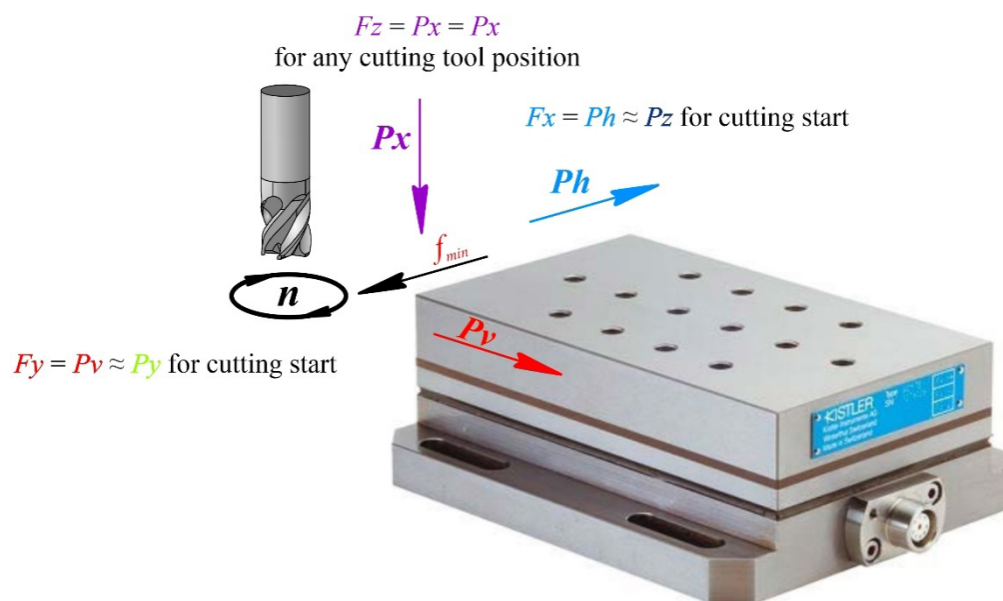


Fig. 9. Flow pattern of cutting forces on the mill relative to the coordinate system of the dynamometer



first symbols in order  $F_z$ ,  $F_x$ ,  $F_y$ . When milling, it is impossible to measure (isolate) with a dynamometer the tangential  $P_z$  and radial  $P_y$  cutting forces acting on the tooth of the cutter and, accordingly, from the tooth of the cutter to the dynamometer, due to the turn (rotation) of the cutter (Fig. 10).

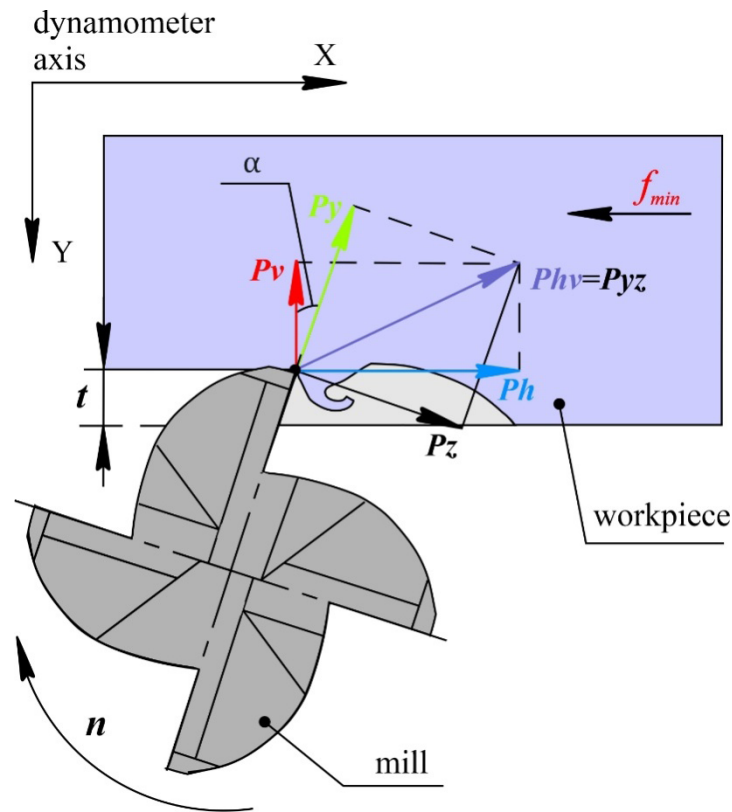


Fig. 10. Scheme of decomposition of cutting forces in a plane perpendicular to the axis of rotation of the mill

During milling, only the forces acting from the cutter on the dynamometer can be measured: the feed force  $Ph$  acting along the feed direction of the table, and the lateral force  $Pv$  acting perpendicular to the feed direction. In this case, the long side of the dynamometer must be installed strictly perpendicular regarding the direction of the table feed, as shown in Fig. 9 and 10, or strictly parallel to the table feed. The designation of these components depends on the direction of the table feed. When mounting the dynamometer with the long side strictly perpendicular to the longitudinal feed of the table (see Fig. 9 and 10), these components of the cutting force have the following designation (indicated by the second symbols in order):  $F_z = Px$ ,  $F_x = Ph$ ,  $F_y = Pv$ .

With a small cutting depth  $t = 1$  mm and a significantly large mill diameter  $d = 12$  mm ( $t/d$  ratio  $< 0.1$ ) and the direction of the minute table feed  $f_{min}$  across the long side of the dynamometer, these directions correspond to another system of forces acting on the specimen (workpiece) from the side of the milling cutter tooth (indicated by the third symbols in order) at the moment when the milling cutter tooth is embedding in the workpiece:  $F_z = Px = Px$ ,  $F_x = Ph \approx Pz$ ,  $F_y = Pv \approx Py$ . The same colors ( $F_z$  – purple,  $F_x$  – blue,  $F_y$  – red) these forces and graphs of its changes are indicated on the monitor. Turning to the system of forces acting on the specimen (workpiece) from the side of the milling cutter tooth, the following approximations will be used:  $Px = Fz$ ,  $Py \approx Fy$ ,  $Pz \approx Fx$ . Thus, you need to understand that in the interface of the Kistler DynoWare software, at the moment when the cutter tooth is embedding in the workpiece,  $F_z$  means that in fact it is  $Px$ ;  $F_y$  means that in fact it is  $Py$ ;  $F_x$  means that in fact it is  $Pz$ .

The surface roughness of the machined specimens was measured using a profilometer model SJ-210 from Mitutoyo (Japan) (Fig. 11). Measurements were performed on five arbitrary sections on the initial workpiece before milling and after removing a layer with a thickness equal to the width of milling  $B$

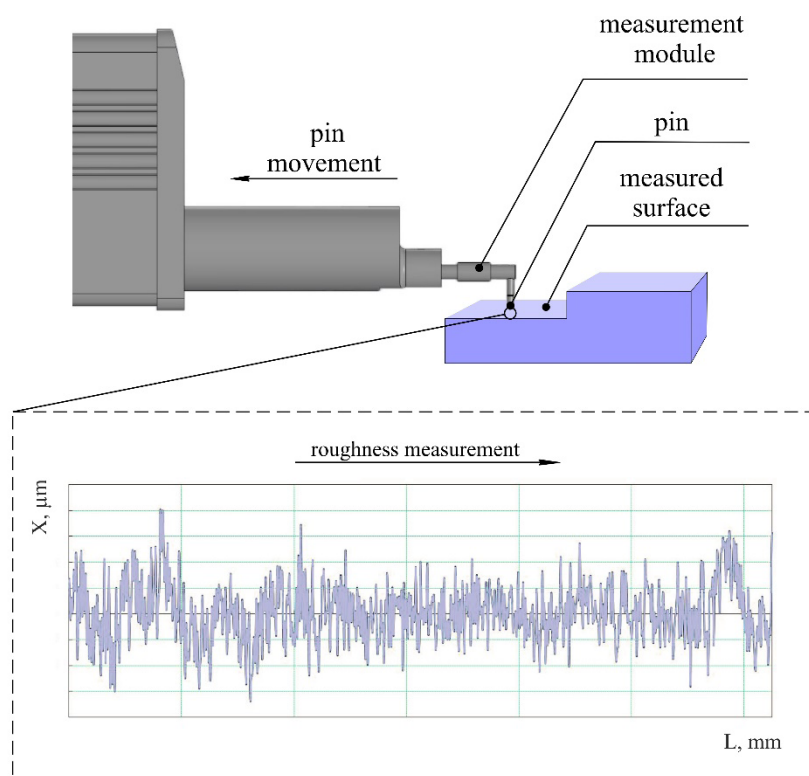


Fig. 11. Process flow diagram of measuring the surface roughness of a specimen after milling

(see Fig. 8). For measurements and data processing of the initial roughness profile, the technique according to *EN ISO 4288* was used.

The data obtained during the registration process were processed using the classical provisions of mathematical statistics and experimental planning, and *STATISTICA* software was used to automate calculations.

## Results and discussion

Below are the results of a study of milling machining of a steel *0.12-Cr18-Ni10-Ti (AISI 321)*.

Measurements of the roughness parameter  $Ra$  depending on the milling modes and the specimens build direction are shown in Table 6.

The milling width was assumed to be  $B = const = 7$  mm with a plate thickness of  $h = 8.5$  mm, i.e. the teeth of the mill at its end were always involved in machining. The minute feed of  $f_{min}$  varied under other identical cutting conditions (machining modes). The least squares method was used to plot graphs based on empirical data.

All figures took into account the changes in the largest magnitude of these forces (see Fig. 12–14).

Graphs of the change in the feed force  $Ph$  (the direction of the force  $Ph$  acts along the feed direction vector) and the lateral force  $Pv$  (the direction of the force  $Pv$  is perpendicular to the direction of the feed vector) with a change in the feed per minute  $f_{min}$  are shown in Fig. 12, and Fig. 13 shows graphs of the change in the axial force  $Px$  (acts along the axis of the mill, i.e. at the end milling – vertically), and for comparison, a graph of the change in the lateral force  $Pv$  is also placed on this field.

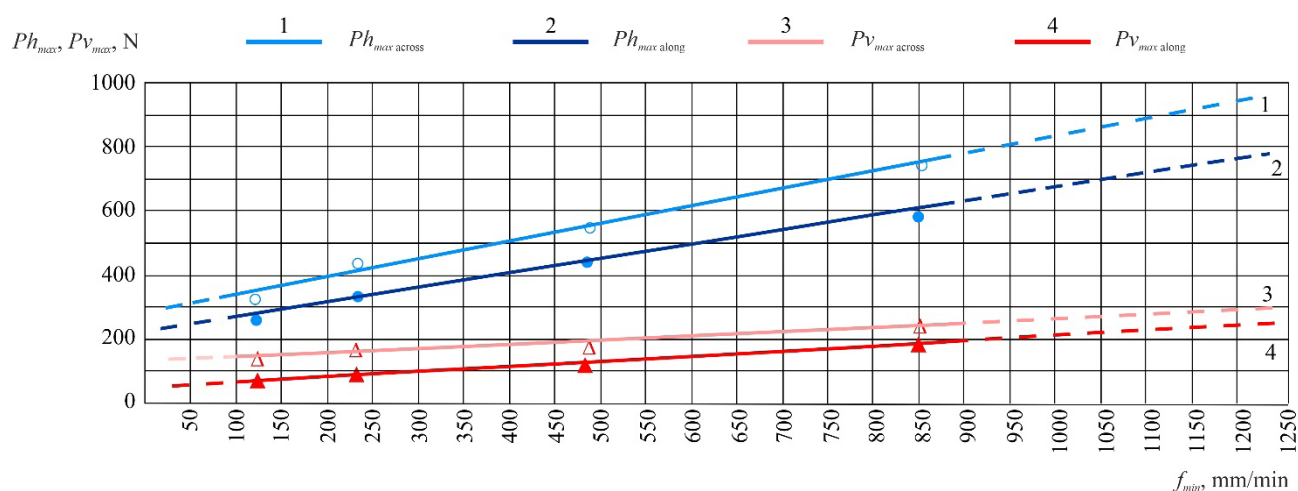
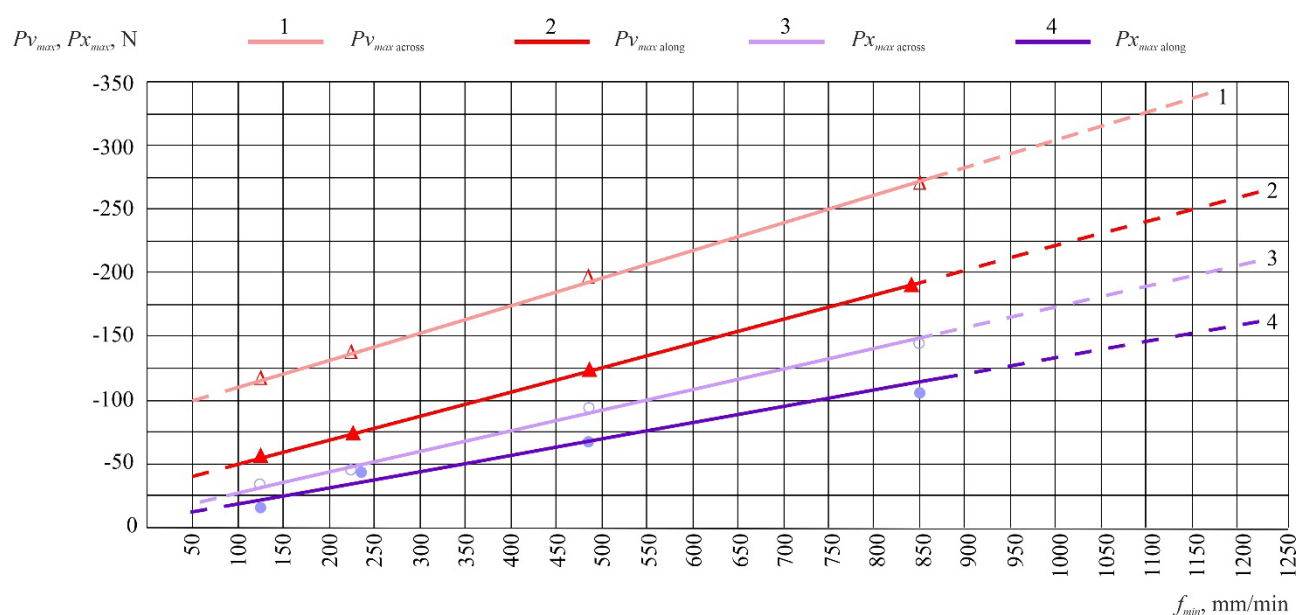
In Fig. 13, the  $Px_{max\ along}$  graph has an inflection when feed  $f_{min} = 240$  mm/min. We believe that it is possible to simplify the nature of this graph and draw a straight line through all four points (line 4 in Fig. 13), taking into account the insignificance of the error under this assumption.

The study of the influence of the milling depth  $t$  on the cutting forces showed a direct proportionality of the forces  $Ph$  from the milling depth (Fig. 15).

Table 6

Roughness values  $Ra$  depending on the milling direction and cutting modes

Experiment No.	$V$ , m/min	$f_{min}$ , mm/min	$t$ , mm	$B$ , mm	$Ra$ , $\mu\text{m}$ (milling along)	$Ra$ , $\mu\text{m}$ (milling across)
1	75	120	1	7	0.817±0,15	2.013±0.24
2		240				1.589±0.15
3		480				1.203±0.20
4		850				0.775±0.24
5	2		0.566±0.20		0.699±0.11	
6	2.5		0.496±0.18		0.566±0.10	
7			94		0.438±0.23	0.510±0.15
8	1.495±0.32	0.922±0.32				
9	1.050	3			1.220±0.22	1.979±0.34

Fig. 12. Graph of changes in the highest values of cutting forces  $Ph$  и  $Pv$  (N) depending on the feed  $f_{min}$  (mm/min) ( $B = 7$  mm,  $V = 75$  m/min,  $t = 1$  mm)Fig. 13. Graph of changes in the highest values of cutting forces  $Ph$  и  $Px$  (N) depending on the feed  $f_{min}$  (mm/min) ( $B = 7$  mm,  $V = 75$  m/min,  $t = 1$  mm)

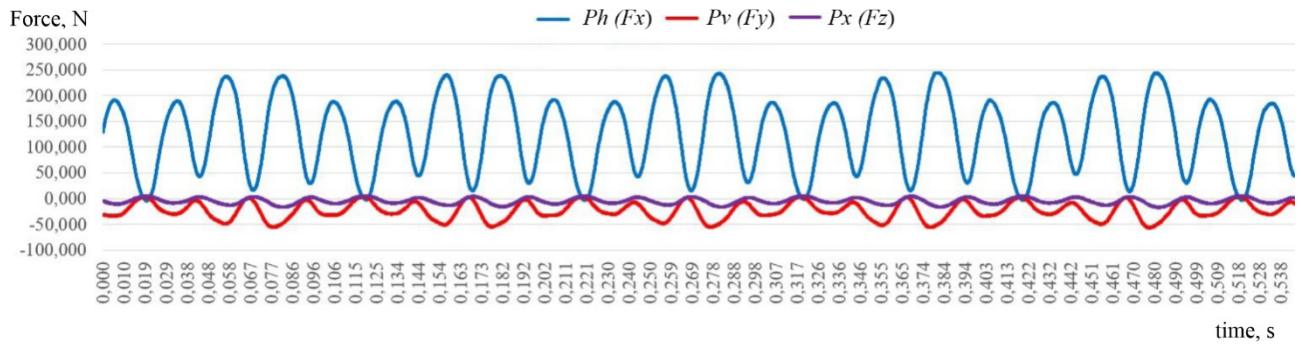


Fig. 14. Example of a graph of changes in the force components from the cutting time in the milling process along the build direction ( $B = 7$  mm,  $V = 75$  m/min,  $t = 1$  mm,  $f_{\min} = 120$  mm/min)

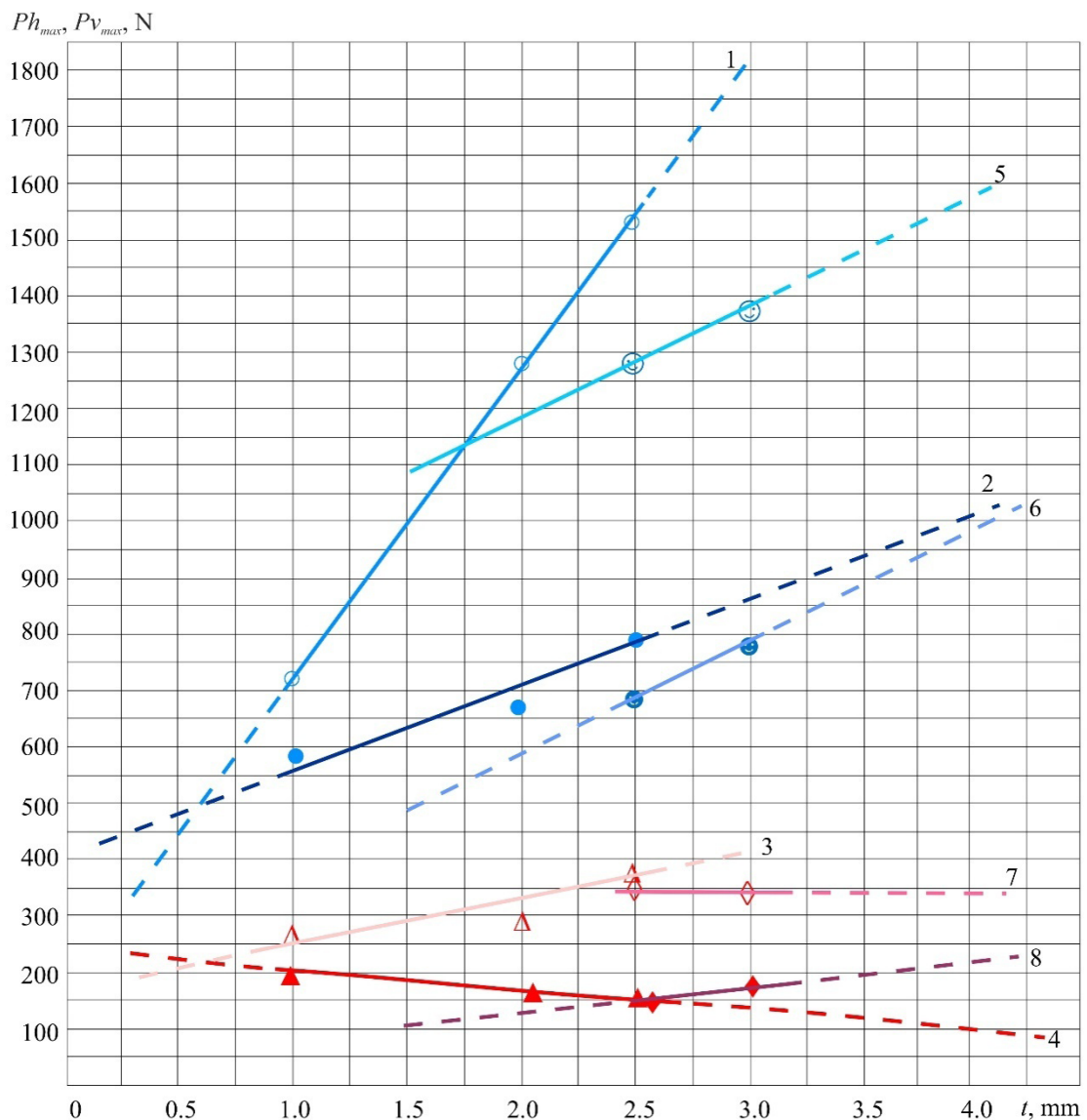
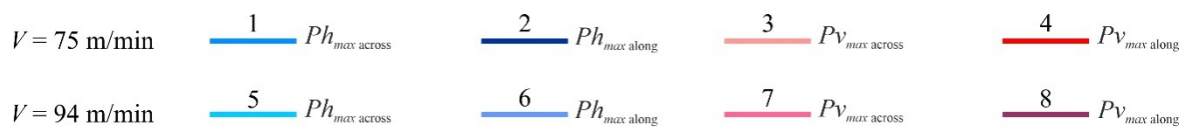


Fig. 15. Components of the cutting force  $Ph$ ,  $Pv$  and  $Px$  (N) when milling in different modes depending on the cutting depth  $t$  (mm) when  $B = 7$  mm



It should be noted that the force  $P_v$  is directed away from the operator, i.e. in the opposite direction of the  $OY$  axis, i.e. the milling cutter tooth pushes the workpiece away from the operator, because when measured, it is displayed on the dynamometer monitor with a minus sign (-). In Fig. 12, the force  $P_v$  is indicated on the positive axis so as not to draw another axis. Despite the negative magnitude of the forces  $P_v$  and  $P_x$ , its absolute value is taken into account – the greater it is, the greater the force.

The sign of the force  $P_h$  is positive, i.e. the direction of the force coincides with the direction of the  $OX$  axis (see Fig. 9). The sign of the force  $P_x$  is negative (-), this indicates that it is directed in the opposite direction from the direction of the  $OZ$  axis, i.e. the milling cutter tooth pulls the workpiece up (see Fig. 9) due to the positive angle of inclination of the screw groove  $\omega$  (see Table 4).

Direct proportionality of graphs  $P_{h_{\max}} = f(f_{\min})$ ,  $P_{v_{\max}} = f(f_{\min})$  from the value of the feed per minute  $f_{\min}$  (see Fig. 12) allows for  $t = 1$  mm and the specified other cutting modes to use equations described by a linear relationship:

$$P_{h_{\max \text{ across}}} = 266.4 + 0.556 \cdot f_{\min}; \quad (1)$$

$$P_{h_{\max \text{ along}}} = 200 + 0.545 \cdot f_{\min}; \quad (2)$$

$$P_{v_{\max \text{ across}}} = 100.4 + 0.899 \cdot f_{\min}; \quad (3)$$

$$P_{v_{\max \text{ along}}} = 46.2 + 0.135 \cdot f_{\min}. \quad (4)$$

Direct proportionality of graphs  $P_{x_{\max}} = f(f_{\min})$  depending on the value of the feed per minute (see Fig. 13) allows for  $t = 1$  mm and the specified other cutting modes to use the equations:

$$P_{x_{\max \text{ across}}} = 10.8 + 0.162 \cdot f_{\min}; \quad (5)$$

$$P_{x_{\max \text{ along}}} = 3.97 + 0.128 \cdot f_{\min}. \quad (6)$$

In all the considered cases, the magnitude of the forces  $P_{h_{\max}}$ ,  $P_{v_{\max}}$  and  $P_{x_{\max}}$  in the feed direction along the feed direction during the synthesis of specimens (workpieces) is slightly less than in the perpendicular feed direction (see Fig. 12 and 13).

The analysis of Fig. 14 shows, despite the fact that at a cutting depth of  $t = 1$  mm, a four-teeth milling cutter should have contact with the specimen of only one tooth and therefore the forces should decrease to zero, but this does not happen. This is most clearly seen in the graphs of changes in the feed force  $P_h$  (blue color of the graph). As the feed increases, the minimum  $P_h$  value increases. In all cases, four peaks and troughs (valleys) are clearly visible, which indicates the operation of four teeth. The different magnitude of these peaks indicates the presence of a small radial runout of the teeth. For the milling cutter used, any two adjacent teeth have the same distance from the axis of rotation of the milling cutter, as indicated by the same magnitude of the greatest  $P_h$  force. This indicates that there is a slightly different distance of the cutting edge of the teeth relative to the axis of rotation of the spindle, and not the displacement of the axis of the cutter when it is fixed in the collet chuck. I.e., the observed error appeared during the manufacture of the milling cutter, and not when it is installed in the chuck.

The steepness of the rise and fall of the force  $P_h$  graph, as the most characteristic, clearly visible and important, is approximately the same (see Fig. 12, 13), although it was expected that the decrease should occur more quickly, because during conventional milling, the tooth exit has a very short exit period (the uncut chip thickness  $a_i$  decreases more quickly before the tooth completely leaves contact with the specimen) compared to the period of increasing the uncut chip thickness.

We explain this phenomenon by changing the direction of the force  $P_z$  as the main force when removing the allowance. Before the tooth leaves the contact, the force  $P_z$  rotates along the rotation of the cutter and increases the force  $P_v$  to a greater extent, rather than the  $P_h$  (see Fig. 12). Therefore, the decrease in the

force  $Ph$  does not occur so quickly, because this decrease begins earlier, even before the tooth approaches the exit point of the main cutting edge from the contact.

In addition, the cutter has a slope of the cutting edge with an angle of  $\omega$  (in some foreign sources this angle is indicated by the symbol  $\beta$ ), which makes it impossible for the entire cutting edge to come out of contact with the workpiece at the same time. And the larger the milling width  $B$  and the larger the angle  $\omega$ , the smoother the reduction of all forces will be.

The rotation of the force vectors  $P_z$  and  $P_y$  during the rotation of the milling cutter with a simultaneous increase in the uncut chip thickness  $a_i$  during conventional milling leads to a slight discrepancy in the phases of changes in the forces  $Ph$  and  $Pv$  (see Fig. 14).

When the cutting speed is increased from 75 to 94 m/min with the same feed  $f_{min}$  feed force  $Ph_{max\ along}$  and  $Ph_{max\ across}$  is less (see Fig. 15, compare graphs 1 and 5; 2 and 6). An increase in the milling depth  $t$  at  $V = 75$  m/min leads to a less significant increase in the force  $Pv_{max\ across}$  (see Fig. 15, graph 3), and the force  $Pv_{max\ along}$  at  $V = 75$  m/min even decreases slightly (see Fig. 15, graph 4), although the forces  $Pv_{max\ along}$  and  $Pv_{max\ across}$  at different speeds differ a little from each other (see Fig. 15, compare graphs 4 and 6; 3 and 7).

At a cutting speed of  $V = 94$  m/min, the force  $Pv$  during milling in the transverse direction relative to the feed direction during AT synthesis ( $Pv_{max\ across}$ ) does not change with increasing milling depth  $t$  (see Fig. 15, graph 7). In the longitudinal feed direction, the force  $Pv_{max\ along}$  does not practically change with increasing cutting depth  $t$  and slightly depends on the cutting speed (see Fig. 15, graphs 4 and 8). This lack of influence of the milling depth  $t$  is explained by an increase in the force  $Pv$  already towards the operator at the last stage of cutting when turning the milling cutter, i.e. the tooth of the cutter begins to pull the workpiece towards the operator, and not push it away as in the initial stage.

Only the force  $Ph_{max\ across}$  decreases significantly with increasing cutting speed  $V$  (see Fig. 15, graphs 1 and 5), and the force  $Ph_{max\ along}$  decreases slightly (see Fig. 15, graphs 2 and 6), and the remaining components of  $Pv_{max\ along}$  and  $Pv_{max\ across}$  (see Fig. 15, graphs 4 and 8, 3 and 7),  $Px_{max\ along}$  and  $Px_{max\ across}$  (graphs are not presented due to the absence of changes in the magnitude of these forces with increasing cutting speed) do not change. It is possible that with a significantly higher cutting speed (more than 130 m/min), the forces will decrease, as is observed when turning in the absence of an built-up edge due to an increase in the deformation rate in the zone of primary plastic deformation and a decrease in plasticity as opposed to an increase in the plasticity of the machined metal due to an increase in temperature [30]. An increase in the deformation rate leads to a decrease in the ductility of the metal and, as a result, to a decrease in the zone of primary plastic deformation, which causes a decrease in the cutting force.

## Conclusion

During the preparation and during the execution of this study, it was possible to minimize the influence of third-party factors on the results due to a comprehensive study of both the parameters of the specimen and the tool, and the conditions of the technological environment for milling. Based on the performed research, the following conclusions are made:

1. The limiting milling modes have been determined, which ensure the absence of destruction of carbide cutters in the process of edge cutting (subtractive) machining of LMD steel 0.12-Cr18-Ni10-Ti (AISI 321), both along and across the growing direction.

2. When studying the cutting forces, it was found that an increase in the feed  $f_{min}$  in the range from 120 to 850 mm/min leads to a directly proportional increase in the forces  $Ph_{max}$ ,  $Pv_{max}$  and  $Px_{max}$  described by linear equations.

3. An increase in the milling depth  $t$  by 2.5 times leads to a significant increase in the feed force  $Ph_{max}$ , especially  $Ph_{max\ across}$  up to 1,580 N, but at the same time the milling depth does not significantly affect the change in lateral and axial forces.

4. The roughness  $Ra$  of the machined surface depends on the direction of growing the additive specimen (workpiece), and when milling in modes (see Table 5) it depends more on the feed and cutting speed. At the same time, the lowest values of  $Ra = 0.438 \pm 0.23$   $\mu\text{m}$  (when milling along) and  $Ra = 0.510 \pm 0.15$   $\mu\text{m}$  (when milling across) are observed in the modes  $V = 94$  m/min;  $f_{min} = 850$  mm/min;  $t = 2.5$  mm;  $B = 7$  mm.



## References

1. Gibson I., Rosen D., Stucker B. *Additive manufacturing technologies*. 2nd ed. New York, Springer Science+Business Media, 2015. 498 p. DOI: 10.1007/978-1-4939-2113-3 (Russ. ed.: Gibson Ya., Rozen D., Staker B. *Tekhnologii additivnogo proizvodstva*. Moscow, Tekhnosfera Publ., 2022. 648 p. ISBN 978-5-94836-447-6).
2. Malakizadi A., Mallipeddi D., Dadbakhsh S., M'Saoubi R., Krajnik P. Post-processing of additively manufactured metallic alloys – A review. *International Journal of Machine Tools and Manufacture*, 2022, vol. 179 (8). DOI: 10.1016/j.ijmachtools.2022.103908.
3. Shiyas K.A., Ramanujam R. A review on post processing techniques of additively manufactured metal parts for improving the material properties. *Materials Today: Proceedings*, 2021, vol. 46 (2), pp. 1429–1436. DOI: 10.1016/j.matpr.2021.03.016.
4. Hällgren S., Pejryd L., Ekengren J. Additive manufacturing and high speed machining – Cost comparison of short lead time manufacturing methods. *Procedia CIRP*, 2016, vol. 50, pp. 384–389. DOI: 10.1016/j.procir.2016.05.049.
5. Bajaj P., Hariharan A., Kini A., Kürnsteiner P., Raabe D., Jäggle E.A. Steels in additive manufacturing: A review of their microstructure and properties. *Materials Science and Engineering A*, 2020, vol. 772 (4). DOI: 10.1016/j.msea.2019.138633.
6. Fousová M., Vojtěch D., Kubásek J., Dvorský D., Machová M. 3D printing as an alternative to casting, forging and machining technologies? *Manufacturing Technology*, 2015, vol. 15 (5), pp. 809–814. DOI: 10.21062/ujep/x.2015/a/1213-2489/MT/15/5/809.
7. Uhlmann E., Rasper P. Influences on specific cutting forces and their impact on the stability behaviour of milling processes. *Production Engineering Research and Development*, 2011, vol. 5, pp. 175–181. DOI: 10.1007/s11740-010-0296-4.
8. Fuchs C., Fritz C., Zaeh M.F. Impact of wire and arc additively manufactured workpiece geometry on the milling process. *Production Engineering Research and Development*, 2023, vol. 17, pp. 415–424. DOI: 10.1007/s11740-022-01153-8.
9. Herzog D., Seyda V., Wycisk E., Emmelmann C. Additive manufacturing of metals. *Acta Materialia*, 2016, vol. 117, pp. 371–392. DOI: 10.1016/j.actamat.2016.07.019.
10. Song Y.-A., Park S., Choi D., Jee H. 3D welding and milling: Part I – A direct approach for freeform fabrication of metallic prototypes. *International Journal of Machine Tools and Manufacture*, 2005, vol. 45 (9), pp. 1057–1062. DOI: 10.1016/j.ijmachtools.2004.11.021.
11. Stucker B., Qu X. A finish machining strategy for rapid manufactured parts and tools. *Rapid Prototyping Journal*, 2003, vol. 9 (4), pp. 194–200. DOI: 10.1108/13552540310489578.
12. Klocke F., Lung D., Buchkremer S., Jawahir I.S. From orthogonal cutting experiments towards easy-to-implement and accurate flow stress data. *Materials and Manufacturing Processes*, 2013 vol. 28 (11), pp. 1222–1227. DOI: 10.1080/10426914.2013.811738.
13. Gu D.D., Meiners W., Wissenbach K., Poprawe R. Laser additive manufacturing of metallic components: materials, processes and mechanisms. *International Materials Reviews*, 2012 vol. 57 (3), pp. 133–164. DOI: 10.1179/1743280411Y.0000000014.
14. Lopes J.G., Machado C.M., Duarte V.R., Rodrigues T.A., Santos T.G., Oliveira J.P. Effect of milling parameters on HSLA steel parts produced by Wire and Arc Additive Manufacturing (WAAM). *Journal of Manufacturing Processes*, 2020, vol. 59, pp. 739–749. DOI: 10.1016/j.jmapro.2020.10.007.
15. Guo P., Zou B., Huang C., Gao H. Study on microstructure, mechanical properties and machinability of efficiently additive manufactured AISI 316L stainless steel by high-power direct laser deposition. *Journal of Materials Processing Technology*, 2017, vol. 240, pp. 12–22. DOI: 10.1016/j.jmatprotec.2016.09.005.
16. Bai Y., Zhao C., Yang J., Hong R., Weng C., Wang H. Microstructure and machinability of selective laser melted high-strength maraging steel with heat treatment. *Journal of Materials Processing Technology*, 2021, vol. 288. DOI: 10.1016/j.jmatprotec.2020.116906.
17. Feldhausen T., Raghavan N., Saleeby K., Love L., Kurfess T. Mechanical properties and microstructure of 316L stainless steel produced by hybrid manufacturing. *Journal of Materials Processing Technology*, 2021, vol. 290. DOI: 10.1016/j.jmatprotec.2020.116970.
18. Kaynak Y., Kitay O. Porosity, surface quality, microhardness and microstructure of selective laser melted 316L stainless steel resulting from finish machining. *Journal of Manufacturing and Materials Processing*, 2018, vol. 2. DOI: 10.3390/jmmp2020036.
19. Struzikiewicz G., Zębala W., Matras A., Machno M., Ślusarczyk Ł., Hichert S., Laufer F. Turning research of additive laser molten stainless steel 316L obtained by 3D printing. *Materials*, 2019, vol. 12. DOI: 10.3390/ma12010182.



20. Greco S., Schmidt M., Klauer K., Kirsch B., Aurich J.C. Hybrid manufacturing: influence of material properties during micro milling of different additively manufactured AISI 316L. *Production Engineering Research and Development*, 2022, vol. 16, pp. 797–809. DOI: 10.1007/s11740-022-01139-6.
21. Maiss O., Grove T., Denkena B. Influence of asymmetric cutting edge roundings on surface topography. *Production Engineering Research and Development*, 2017, vol. 11, pp. 383–388. DOI: 10.1007/s11740-017-0742-7.
22. Yang N., Yee J., Zheng B., Gaiser K., Reynolds T., Clemon L., Lu W.Y., Schoenung J.M., Lavernia E.J. Process-structure-property relationships for 316L stainless steel fabricated by additive manufacturing and its implication for component engineering. *Journal of Thermal Spray Technology*, 2017, vol. 26, pp. 610–626. DOI: 10.1007/s11666-016-0480-y.
23. Yang Y., Gong Y., Qu S., Xin B., Xu Y., Qi Y. Additive/subtractive hybrid manufacturing of 316L stainless steel powder: Densification, microhardness and residual stress. *Journal of Mechanical Science and Technology*, 2019, vol. 33, pp. 5797–5807. DOI: 10.1007/s12206-019-1126-z.
24. Aqilah D.N., Sayuti A.K.M., Farazila Y., Suleiman D.Y., Amirah M.A.N., Izzati W.B.W.N. Effects of process parameters on the surface roughness of stainless steel 316L parts produced by selective laser melting. *ASTM International Journal of Testing and Evaluation*, 2018, vol. 46 (4), pp. 1673–1683. DOI: 10.1520/JTE20170140.
25. Liao Z., Monaca A., Murray J., Speidel A., Ushmaev D., Clare A., Axinte D., M'Saoubi R. Surface integrity in metal machining – Part I: Fundamentals of surface characteristics and formation mechanisms. *International Journal of Machine Tools and Manufacture*, 2021, vol. 162. DOI: 10.1016/j.ijmachtools.2020.103687.
26. Mohd Yusuf S., Cutler S., Gao N. Review: the impact of metal additive manufacturing on the aerospace industry. *Metals*, 2019, vol. 9 (12), p. 1286. DOI: 10.3390/met9121286.
27. Luecke W.E., Slotwinski J.A. Mechanical properties of austenitic stainless steel made by additive manufacturing. *Journal of Research of the National Institute of Standards and Technology*, 2014, vol. 119, pp. 398–418. DOI: 10.6028/jres.119.015.
28. Shrestha R., Simsiriwong J., Shamsaei N. Fatigue behavior of additive manufactured 316L stainless steel parts: Effects of layer orientation and surface roughness. *Additive Manufacturing*, 2019, vol. 28, pp. 23–38. DOI: 10.1016/j.addma.2019.04.011.
29. Kok Y., Tan X.P., Wang P., Nai M.L.S., Loh N.H., Liu E., Tor S.B. Anisotropy and heterogeneity of microstructure and mechanical properties in metal additive manufacturing: A critical review. *Materials & Design*, 2018, vol. 139, pp. 565–586. DOI: 10.1016/j.matdes.2017.11.021.
30. Kozlov V., Babaev A., Schulz N., Semenov A., Shevchuk A. Study of a methodology for calculating contact stresses during blade processing of structural steel. *Metals*, 2023, vol. 13, p. 2009. DOI: 10.3390/met13122009.
31. Kluczyński J., Śniezek L., Grzelak K., Janiszewski J., Płatek P., Torzewski J., Szachogłuchowicz I., Gocman K. Influence of selective laser melting technological parameters on the mechanical properties of additively manufactured elements using 316L austenitic steel. *Materials*, 2020, vol. 13, p. 1449. DOI: 10.3390/ma13061449.

## Conflicts of Interest

The authors declare no conflict of interest.

© 2024 The Authors. Published by Novosibirsk State Technical University. This is an open access article under the CC BY license (<http://creativecommons.org/licenses/by/4.0>).